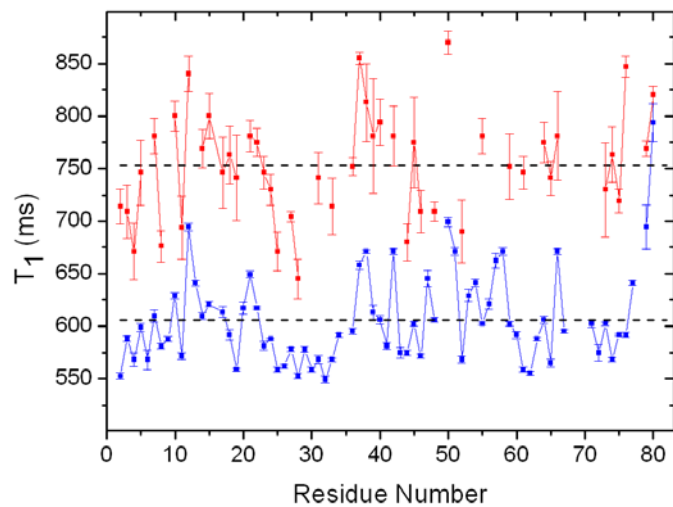
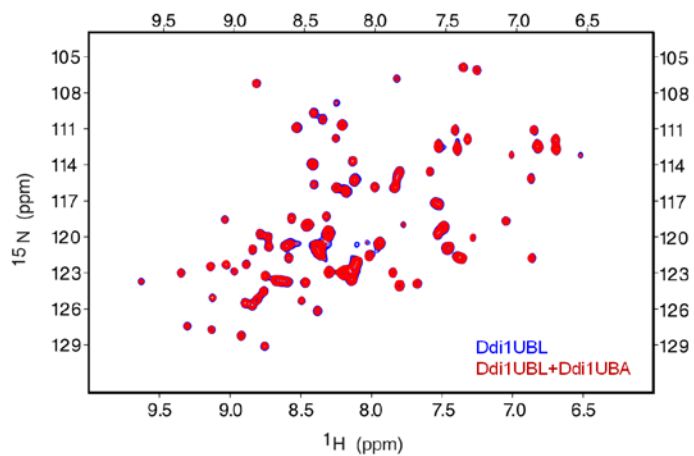
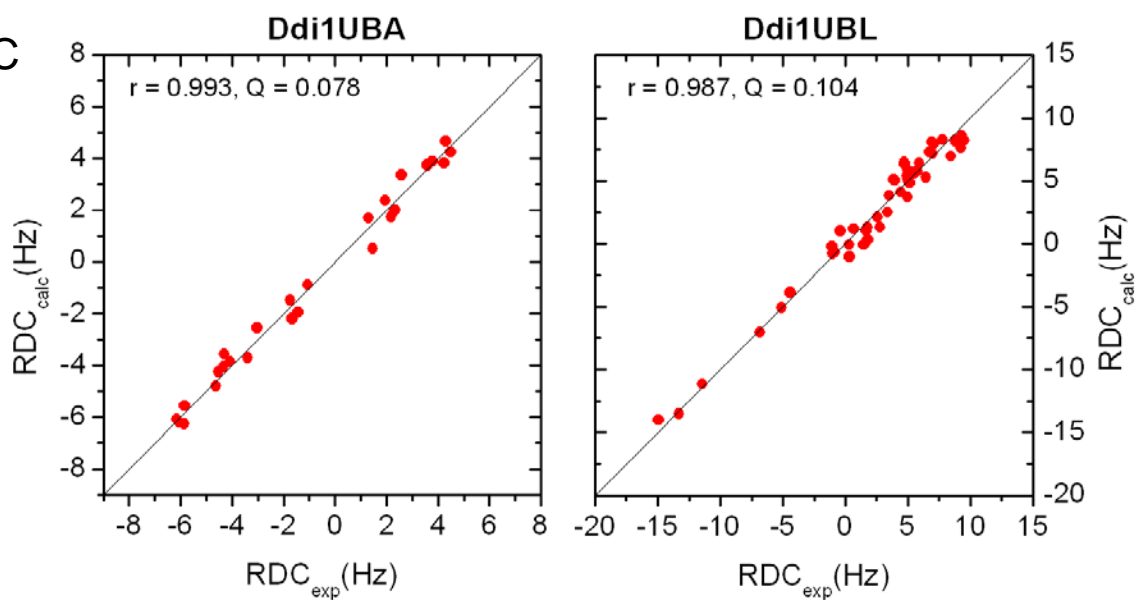


## Supplemental Figures



Figure S1, related to Figure 1. Sequence analysis and conservation of the UBA and UBL domains of Ddi1. Sequence alignment of (A) Ddi1UBA domain with the UBA domains of other shuttle proteins (Dsk2 and Rad23) from yeast and (B) of Ddi1UBL domain with Ub (yeast and human) and the UBL domains of Rad23 and Dsk2 from yeast. (C) Domain composition of Ddi1, Dsk2, and Rad23 from *Saccharomyces cerevisiae*. (D) Quantification of the sequence comparison between the indicated UBL or UBA domains.

**A****B****C**

D



|             | Dsk2 UBA | hhR23A UBA1 | hhR23A UBA2 | Mud1 UBA | UQ1 UBA | Ddi1 UBA | PDB ID            |
|-------------|----------|-------------|-------------|----------|---------|----------|-------------------|
| Dsk2 UBA    |          |             |             |          |         |          | 2BWB              |
| hhR23A UBA1 | 1.481    |             |             |          |         |          | 1IFY              |
| hhR23A UBA2 | 0.751    | 1.294       |             |          |         |          | 1DV0              |
| Mud1 UBA    | 0.989    | 1.066       | 0.743       |          |         |          | 1Z96              |
| UQ1 UBA     | 1.392    | 1.840       | 1.675       | 1.506    |         |          | 2JY5              |
| Ddi1 UBA    | 1.251    | 0.866       | 1.269       | 0.886    | 1.622   |          | 2MR9<br>this work |

E

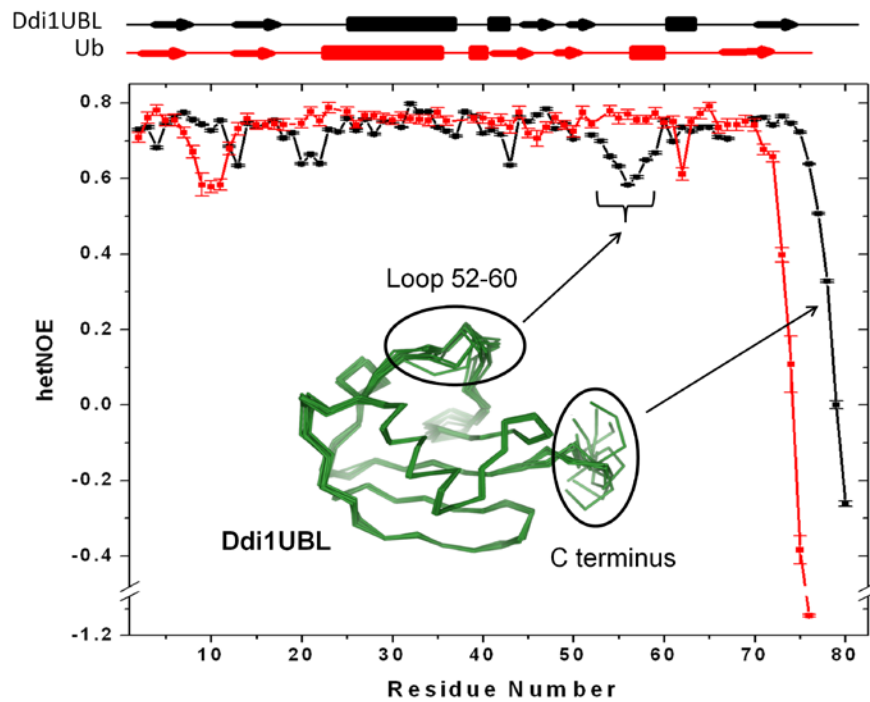


Figure S2, related to Figure 2. (A)  $^{15}\text{N}$  longitudinal relaxation time ( $T_1$ ) for backbone amides in the UBL domain of Ddi1 as an isolated domain (blue) and as part of the full-length Ddi1 construct (red). Shown for the full-length construct are only data for those residues that were assigned with confidence. The dashed line indicates the average  $T_1$  value,  $606 \pm 44$  ms for the isolated UBL domain and  $753 \pm 51$  ms in the context of full-length Ddi1. If the UBL domain in Ddi1 was tumbling together with the rest of this 47 kDa protein, the expected  $T_1$  would have been  $\sim 1650$  ms, according to  $T_1$ 's molecular weight dependence (Varadan et al., 2005b). These  $T_1$  values were measured at magnetic field of 14.1 T ( $^1\text{H}$  frequency 600 MHz).

(B) Overlay of  $^1\text{H}$ - $^{15}\text{N}$  SOFAST-HMQC spectra of [ $^{15}\text{N}$ ,  $^{13}\text{C}$ ]-Ddi1UBL alone (blue) and in the presence of Ddi1UBA (red) at 1:1 molar ratio. The almost perfect overlay of the two spectra indicates that Ddi1UBL does not interact with Ddi1UBA, at least at the conditions used here.

(C) The agreement between the experimental RDCs and their back-calculated values from the derived structures for Ddi1UBA (left) and Ddi1UBL (right). The values of the Pearson's correlation coefficient  $r$  and the quality factor  $Q$  (Clare and Garrett, 1999) are indicated. Low  $Q$  values indicate good agreement with experiment.

(D) Comparison of the 3-D structures of Ddi1UBA and UBA domains from other shuttle proteins. (Top) Superimposition of the structures of Ddi1UBA (green), Dsk2UBA (cyan) and UBA1 of hHR23A (magenta). (Bottom) Backbone ( $\text{C}\alpha$ ) RMSD values (in  $\text{\AA}$ ) between various UBA domains. UQ1 (ubiquilin-1, aka hPLIC-1) is human homologue of Dsk2, hHR23A is human homologue of Rad23A, and Mud1 is *S. pombe* homolog of Ddi1.

(E) Comparison of the steady-state heteronuclear  $^{15}\text{N}\{^1\text{H}\}$ NOE (hetNOE) values for backbone amides in Ddi1UBL (black) and Ub (red): The elements of secondary structure in Ddi1UBL and Ub are indicated on the top. Ddi1UBL residues with low hetNOE values, indicative of high backbone flexibility, are located in the long loop (residues 52-60) and the C terminus, as well as in the loop between strands  $\beta 1$  and  $\beta 2$  and in the loop connecting strand  $\beta 2$  and the  $\alpha$ -helix. These parts of Ddi1UBL structure exhibit significant degree of disorder in the structural ensemble (shown in the center) derived from the NMR data.

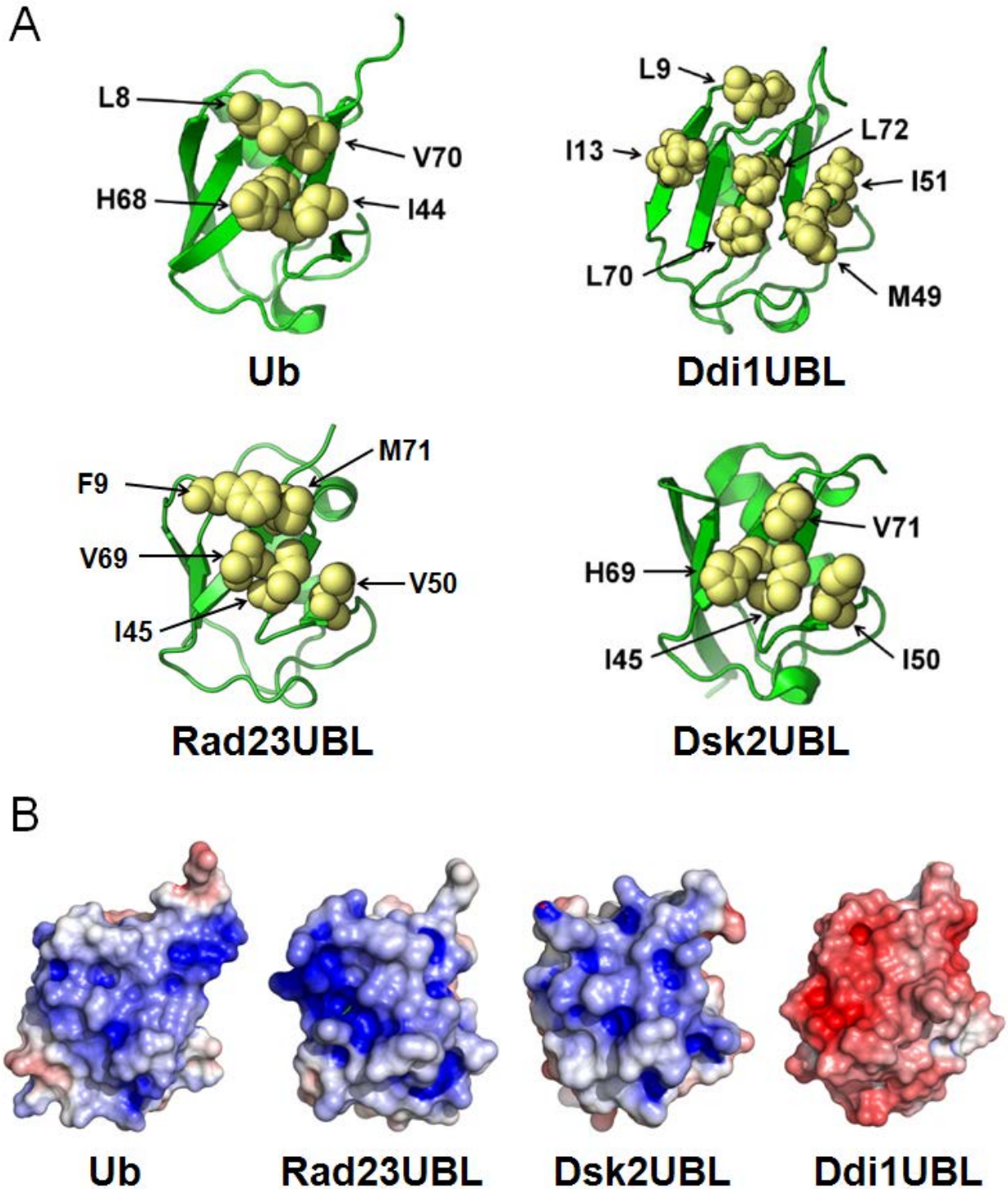


*Figure S3, related to Figure 3.* Comparison of the structure and electrostatic potential of Ub and the UBL domains from yeast proteasomal shuttle proteins Ddi1, Rad23, and Dsk2. (A) Solvent-exposed hydrophobic residues on the  $\beta$ -sheet side of the surface of Ub (PDB ID 1UBQ) and the UBL domains from Ddi1 (this work), Rad23 (PDB ID 3M62), and Dsk2 (PDB ID 2BWF). Backbone structures of Ub, Ddi1, Rad23, and Dsk2 are shown as green ribbons. Hydrophobic

side chains are shown as yellow spheres and indicated with arrows. The backbone RMSD (for secondary structure) between Ddi1UBL and these proteins is 1.92 Å for Ub, 1.96 Å for Rad23 UBL, and 2.06 Å for Dsk2 UBL.

3D-structure-based sequence alignment of Ub and the UBLs in this figure.

```
Ddi1UBL:  MDLTISNELTGEIYGPIEVSEDMALTDLIALLQADCGFDKTKHDLYYNMDILDSNRTQSLKELGLKTDDLLLRGKISNS
Dsk2:      MSLNIHIKSGQDKW-EVNVAPESTVLQFKEAINKANGIPVANQRLIYSGKILKDD--QTVESYHIQDGHVHLVKSQPK-
Rad23:     MVSLTFKN-FKKEKV-PLDLEPSNTILETKTKLAQSISCEESQIKLIYSGKVLQDS--KTVSECGLKDGQVVMVSQKKS
Ub s.c.:   MQIFVKT-LTGKTI-TLEVESSDTIDNVKSKIQDKEGIPPDQQRLLIFAGKQLEDG--RTLSDYNIQKESTLHLVLRRLGG
Ub h.s.:   MQIFVKT-LTGKTI-TLEVEPSDTIENVKAKIQDKEGIPPDQQRLLIFAGKQLEDG--RTLSDYNIQKESTLHLVLRRLGG
```

(B) Surface electrostatic potential of Ub (PDB ID 1D3Z) and the UBL domains from Ddi1 (this work), Rad23 (PDB ID 3M62), and Dsk2 (PDB ID 2BWF). Positive values of the potential are shown in blue while the negative values are red; the range is  $\pm 4$  kT/e for Ub,  $\pm 7$  kT/e for Rad23UBL,  $\pm 6$  kT/e for Dsk2UBL, and  $\pm 8$  kT/e for Ddi1UBL. All molecules are oriented similarly (as shown in A) and such that the  $\beta$ -sheet surface faces the reader. The electrostatic potential map was generated using Adaptive Poisson Boltzmann Solver (APBS) via PDB2PQR web server ([http://nbc222.ucsd.edu/pdb2pqr\\_1.8/](http://nbc222.ucsd.edu/pdb2pqr_1.8/)) (Dolinsky et al., 2004), and visualized using Pymol (Pymol). All calculations were performed using SWANSON force field at pH6.8 and 0 NaCl.

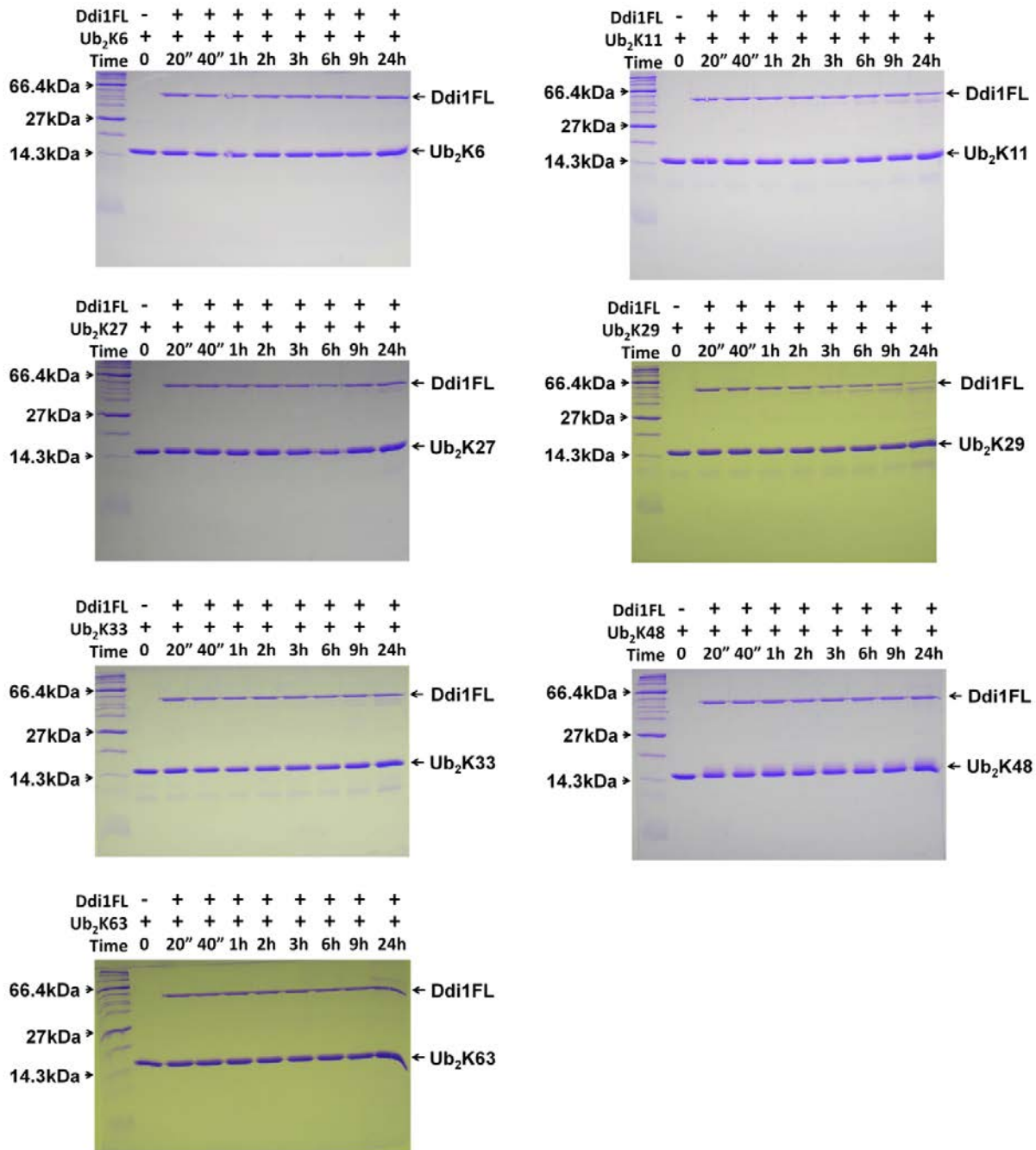


*Figure S4 related to Results.* Time-course of deubiquitination activity assay examining if Ddi1 has a protease/isopeptidase activity against K6-, K11-, K27-, K29-, K33-, K48-, or K63-linked di-ubiquitins. Reaction mixture contained 25  $\mu$ M of a given di-ubiquitin chain and 5  $\mu$ M of FL Ddi1, in 50 mM Tris at pH 8.0. Each reaction was carried out at 30°C. Samples were taken at indicated time points, ran through SDS-PAGE gels, and stained with coomassie blue. No Ddi1FL DUB activity was detected at these experimental conditions.

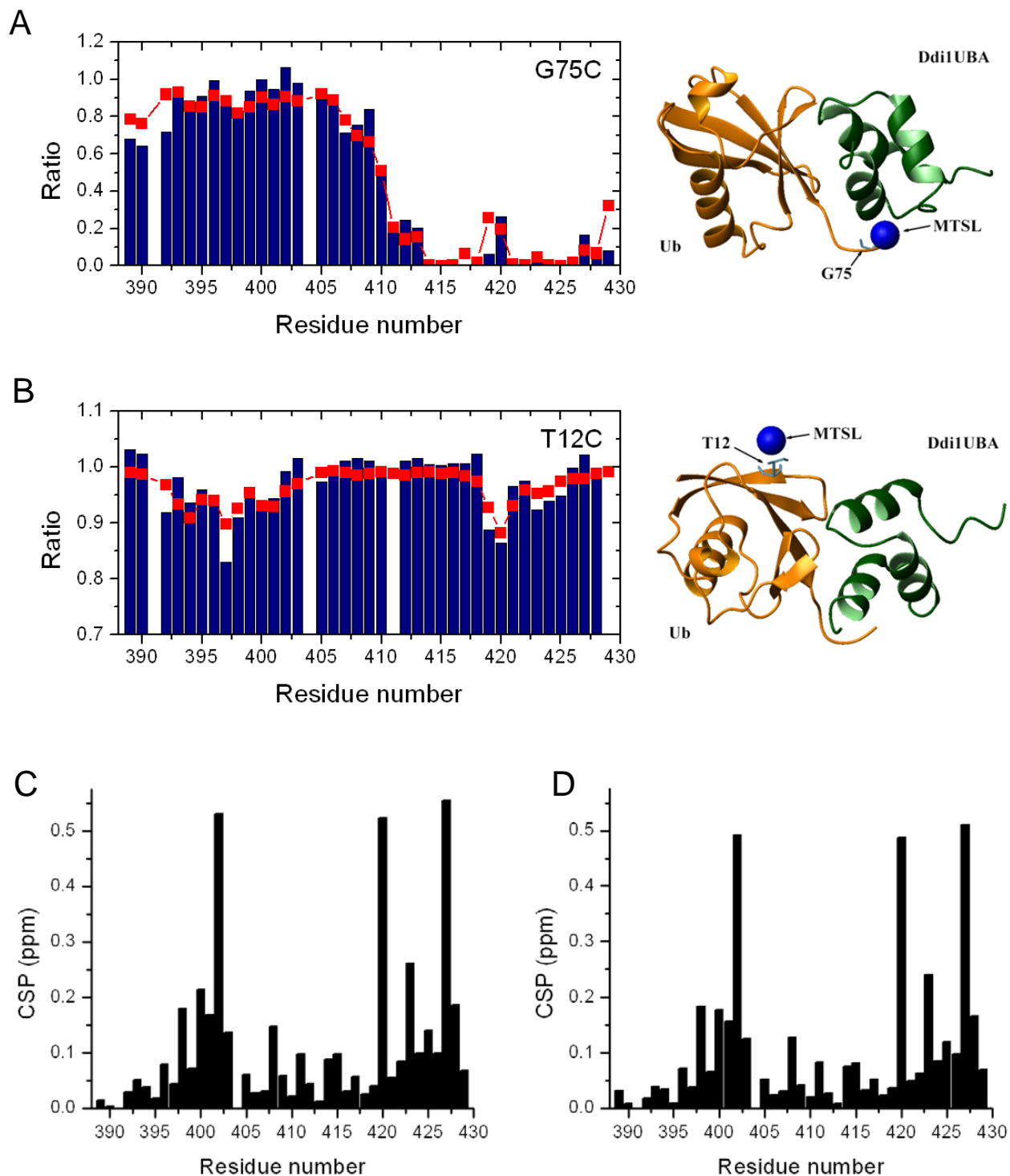


*Figure S5, related to Figure 4. (A-B) Intermolecular distance restraints for the Ub:Ddi1UBA complex calculation were obtained using site-directed paramagnetic spin-labeling. Shown are the results of two independent experiments in which the spin-label (MTSL) was attached to a cysteine residue at position 75 (A) or 12 (B) in Ub (Ub<sup>G75C</sup> or Ub<sup>T12C</sup>, respectively), and the paramagnetic relaxation enhancement (PRE) effects were measured in <sup>15</sup>N-labeled Ddi1UBA.*

The Ub-MTSL:Ddi1UBA molar ratio was 3:1 in (A) and ~0.8:1 in (B). Empty bars correspond to prolines (391 and 404) or residues with signal overlap (411 and 429 in (B)). The left panels show signal attenuations in Ddi1UBA detected experimentally (blue bars) and back-calculated (red squares) based on the atom coordinates of Ddi1UBA and the reconstructed position of MTSL's unpaired electron. Shown on the right is the structure of the Ub:Ddi1UBA complex; the location of MTSL, reconstructed from the PREs detected in Ddi1UBL, is shown as a blue sphere superimposed on the complex structure. The Ub's cysteine to which the MTSL was attached is shown in stick representation and indicated. The position of the MTSL's unpaired electron reconstructed from the PREs measured in Ddi1UBA was used to generate loose intermolecular distance restraints included in the HADDOCK calculation.

(C-D) Ddi1UBA:Ub binding at 150 mM NaCl. Comparison of the CSPs in Ddi1UBA at the endpoint of titration with Ub ([Ub]/[UBA]=8:1) at (C) 0 mM NaCl and (D) 150 mM NaCl. Both studies were performed in 20 mM phosphate buffer, pH 6.8, the starting concentration of Ddi1UBA was 250  $\mu$ M. The average  $K_d$  value was  $137 \pm 12$   $\mu$ M in 0 mM NaCl and  $291 \pm 13$   $\mu$ M in 150 mM NaCl (averaged over 9 residues). Note that the titration at 0 mM NaCl was an independent repeat of that shown in Figure 4 (main text), this time the titration went up to 8:1 molar ratio of Ub to Ddi1UBA. The starting concentration of Ddi1UBA was 250  $\mu$ M.

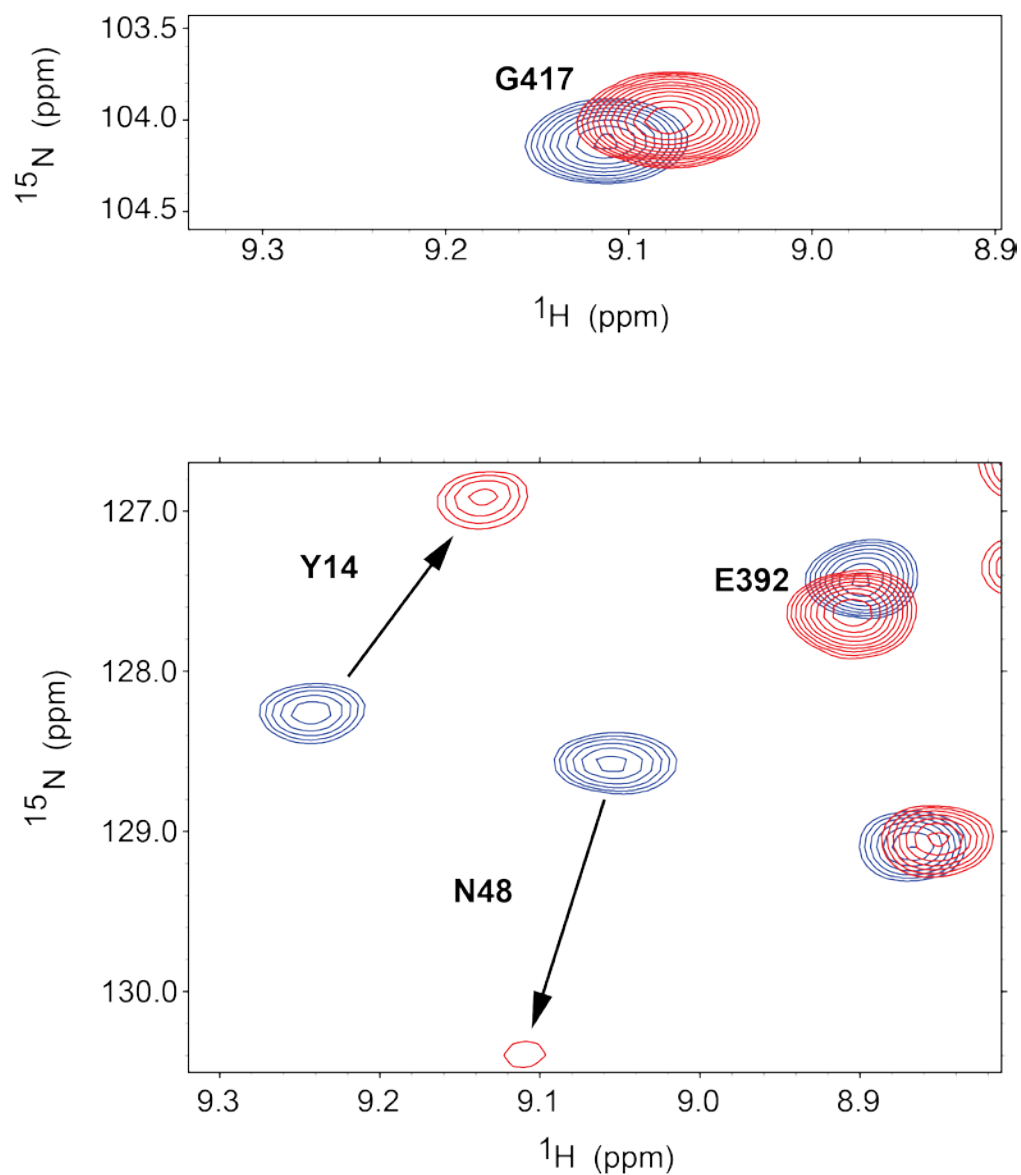
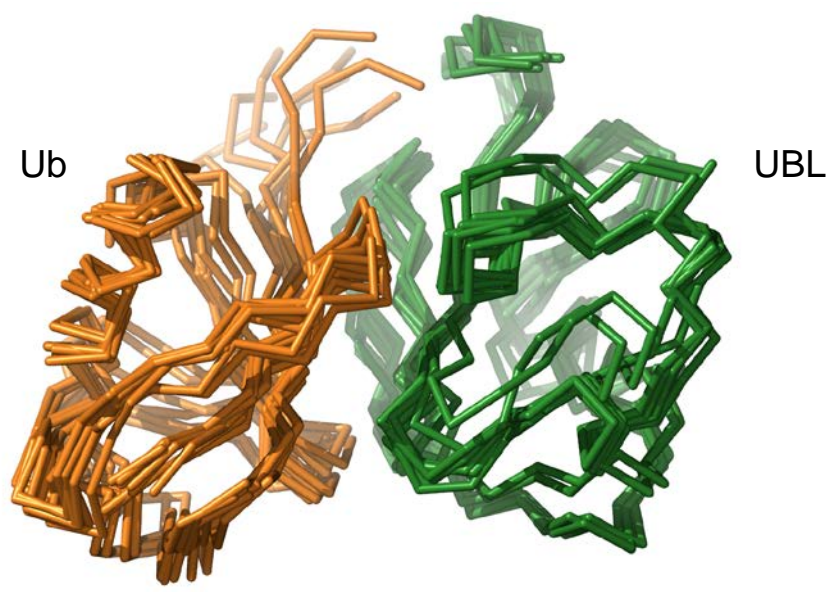
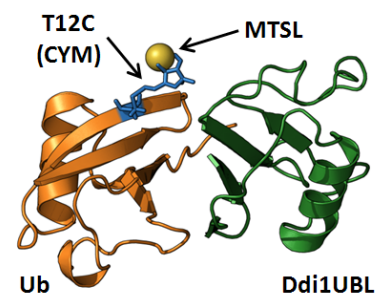
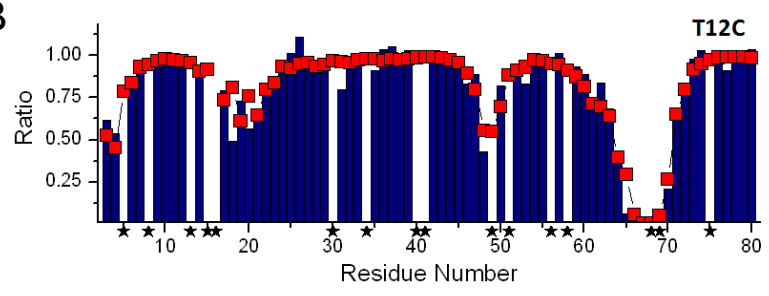


*Figure S6, related to Figure 5.* Comparison of the magnitudes of NMR signal shifts of selected residues in the UBL (Y14, N48)) and UBA (E392, G417) domains in the context of full-length  $^{15}\text{N}$ -labeled Ddi1 upon addition of Ub. Shown is an overlay of the  $^1\text{H}$ - $^{15}\text{N}$  TROSY spectra of full-length Ddi1 alone (blue contours) and in the presence of a 2-fold molar excess of Ub (red contours).

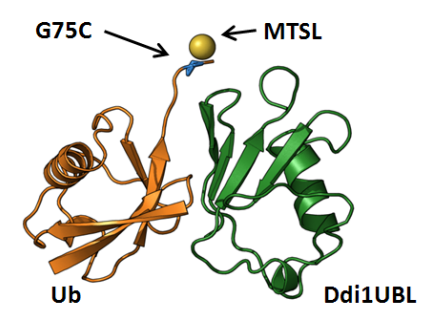
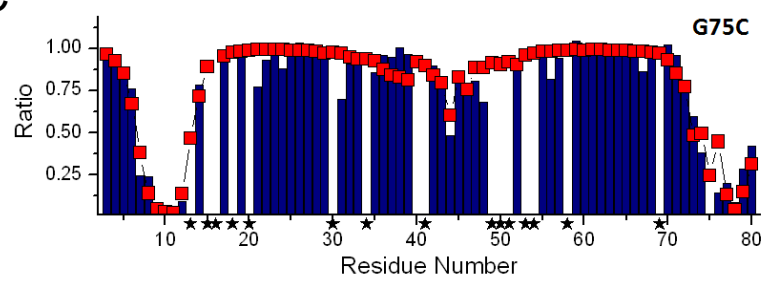
A



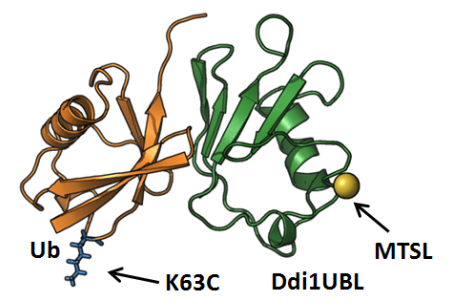
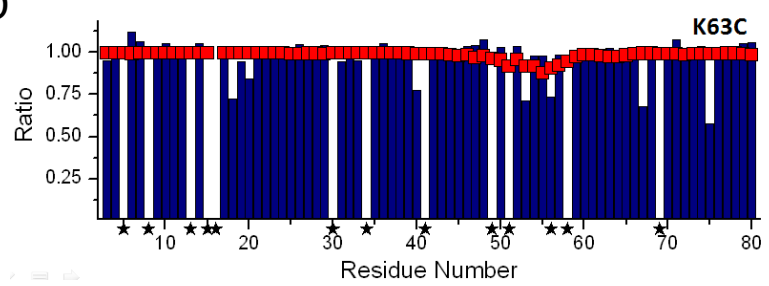
B

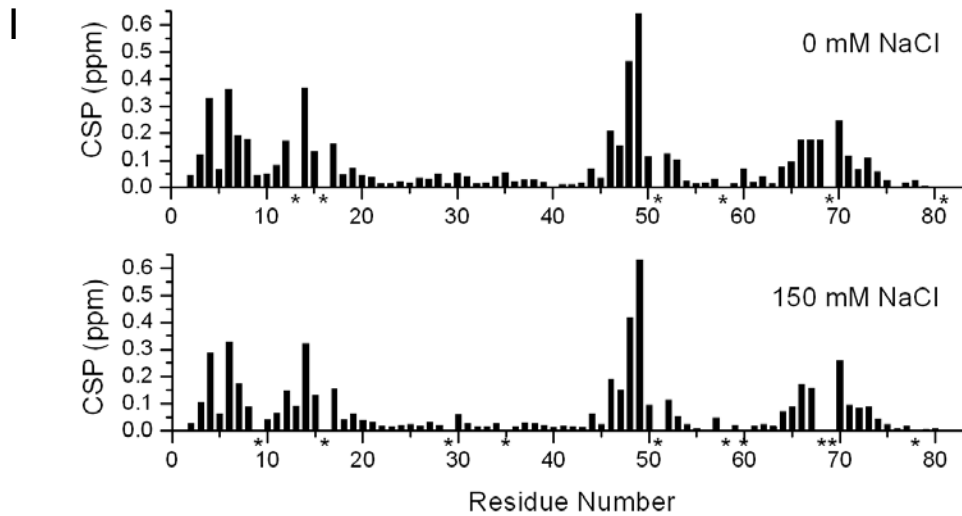
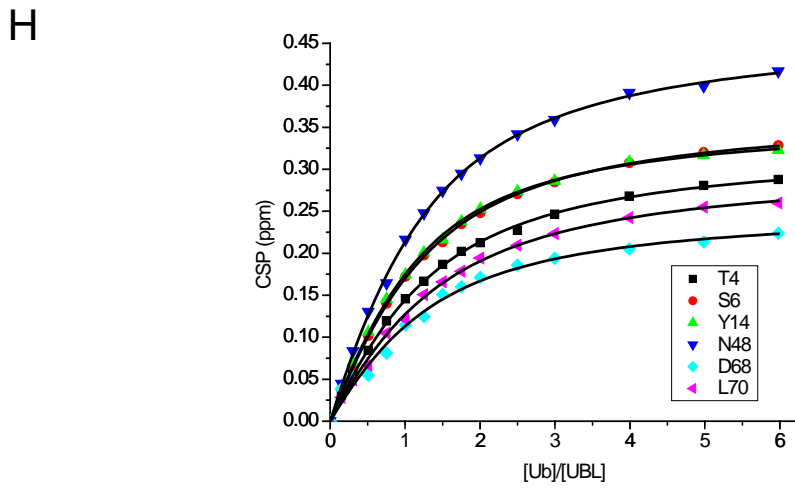
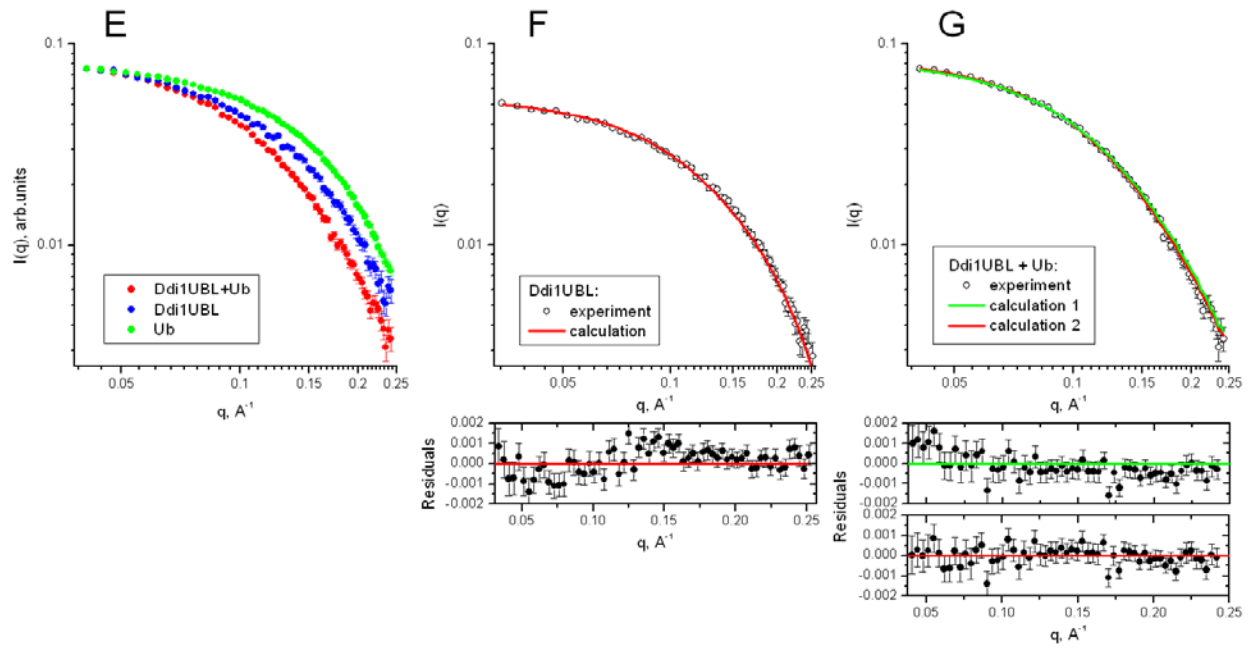


C



D





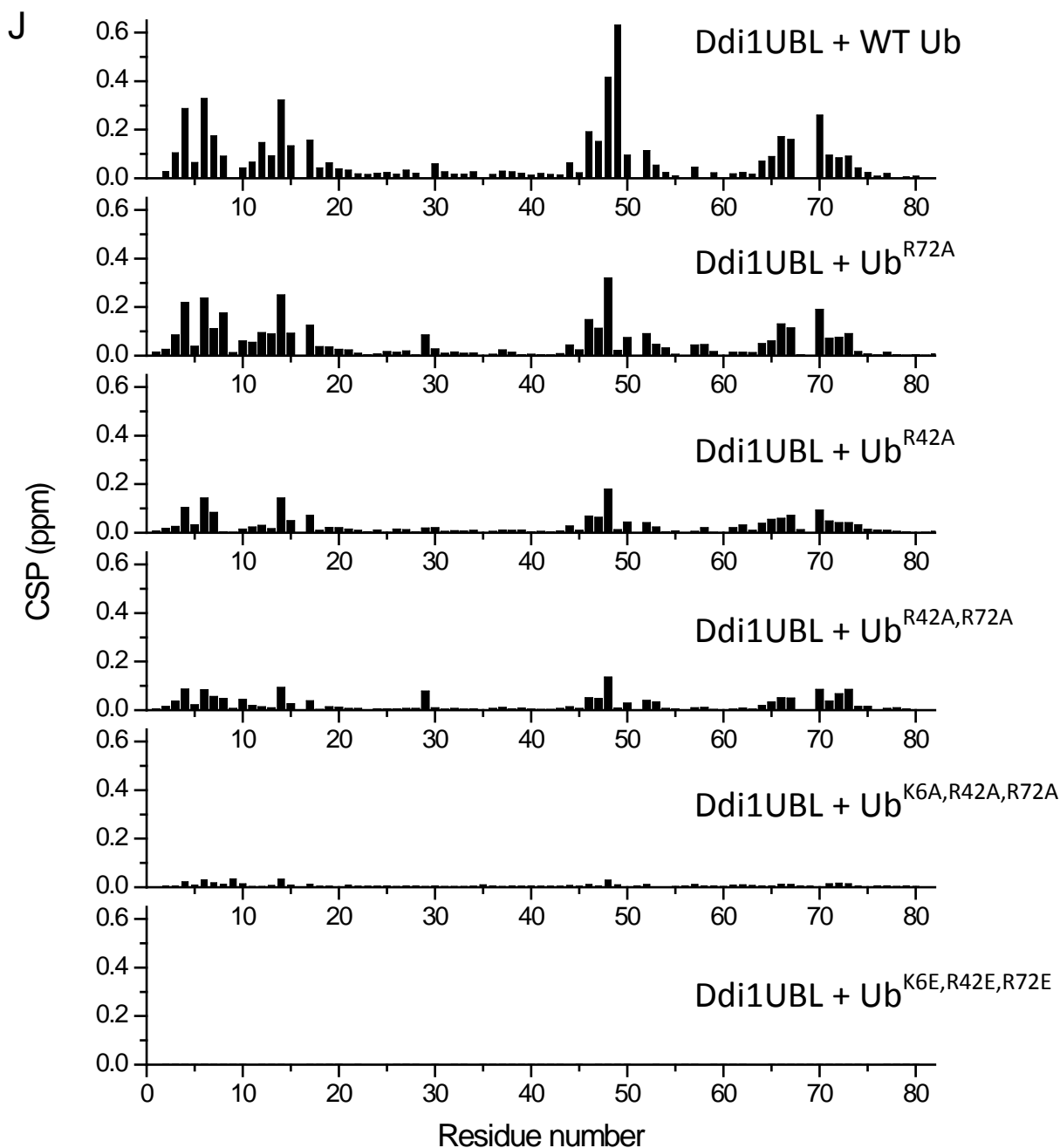


*Figure S7, related to Figures 6 and 7.*

(A) Overlay of eight structures of Ub:Ddi1UBL complex from the top cluster generated by HADDOCK. Shown are backbone traces for Ub (orange) and UBL (green), superimposed by secondary structure elements; the backbone RMSD for the elements of secondary structure is 1.67 Å among all structures in this ensemble, and 1.15 Å to the mean structure.

(B-D) Validation of the NMR-derived structure of Ub:Ddi1UBL complex using site-directed paramagnetic spin-labeling. Shown are the results of three independent experiments in which the spin-label (MTSL) was attached to a cysteine residue at position 12 (B), 75 (C), or 63 (D) in Ub (Ub T12C, Ub G75C, or Ub K63C, respectively), and the paramagnetic relaxation enhancement (PRE) was measured in  $^{15}\text{N}$ -labeled Ddi1UBL. Both proteins were present in equimolar amounts. The left panels show signal attenuations in Ddi1UBL detected experimentally (blue bars) and back-calculated (red squares) based on the Ub:Ddi1UBL complex structure. The residues that were not included in the analysis because of the signal overlap are marked with asterisks. Structures on the right show the position of the spin label's unpaired electron (yellow spheres) reconstructed from the experimental data and the Ddi1UBL coordinates in the complex. The actual cysteine on Ub to which the MTSL is attached is shown in blue sticks.

(E-G) Validation of the NMR-derived structures of Ddi1UBL and Ub:Ddi1UBL complex using small-angle neutron scattering (SANS).

(E) Comparison of the scattering intensities,  $I(q)$ , as a function of the scattering vector  $q$ , measured for isolated Ub (magenta), isolated Ddi1UBL (blue), and for the Ddi1UBL+Ub sample (black). To facilitate the comparison of the scattering profiles, the  $I(q)$  values for Ub and Ddi1UBL were scaled such that their lowest- $q$  values match that of  $I(q)$  for the Ddi1UBL+Ub sample. The vertical bars in all plots throughout this figure represent experimental errors in  $I(q)$ .

(F) (Top) Overlay of the experimental (open circles) and calculated (blue line) values of  $I(q)$  for Ddi1UBL. (Bottom) The corresponding residuals: experiment minus calculation. The residuals are generally within the experimental errors in  $I(q)$ .

(G) (Top) Overlay of the experimental (open circles) and calculated (green and red lines, for calculations 1 and 2, respectively) values of  $I(q)$  for the Ddi1UBL+Ub sample. (Bottom) The corresponding residuals,  $I(q) - I(q)^{total}$ , are shown for calculation 1 (green) and calculation 2 (red). The residuals are generally within the experimental errors in  $I(q)$ . The calculated scattering,  $I(q)^{total}$ , for Ddi1UBL+Ub was computed using Eq (S1) as detailed below in Supplemental Experimental Procedures.

(H-I) Ddi1UBL:Ub binding at 150 mM NaCl. (H) Representative titration curves for selected residues in Ddi1UBL, the lines represent their fit to a 1:1 binding model. The average  $K_d$  value was  $175 \pm 24 \mu\text{M}$  (averaged over 6 residues). (I) Comparison of the CSPs in Ddi1UBL at the endpoint of titration with Ub in the absence (top) and presence of 150 mM NaCl (bottom). Both studies were performed in 20 mM phosphate buffer, pH 6.8. Residues having overlapping signals are indicated with stars. M49 in 150 mM NaCl showed signal broadening and overlap with another signal in the last points in titration.

(J) Mutations of the charged residues at the Ub:Ddi1UBL interface weaken or abolish the Ub:Ddi1UBL interaction. Shown are CSPs as a function of residue number in  $^{15}\text{N}$ -labeled Ddi1UBL upon addition of WT Ub or the indicated Ub mutants. These studies were performed in 20 mM phosphate buffer with 150 mM NaCl, pH 6.8.  $^1\text{H}$ - $^{15}\text{N}$  NMR spectra (not shown)

confirmed that all these Ub variants are well folded and structurally similar to Ub. The  $^{15}\text{N}$   $T_1$  at 18.8 T ( $^1\text{H}$  frequency 800 MHz) was  $771 \pm 46$  ms for Ddi1UBL alone,  $777 \pm 51$  ms for Ddi1UBL+Ub<sup>K6E,R42E,R72E</sup>,  $813 \pm 48$  ms for Ddi1UBL+Ub<sup>K6A,R42A,R72A</sup>, and  $1183 \pm 84$  ms for Ddi1UBL+WT Ub.

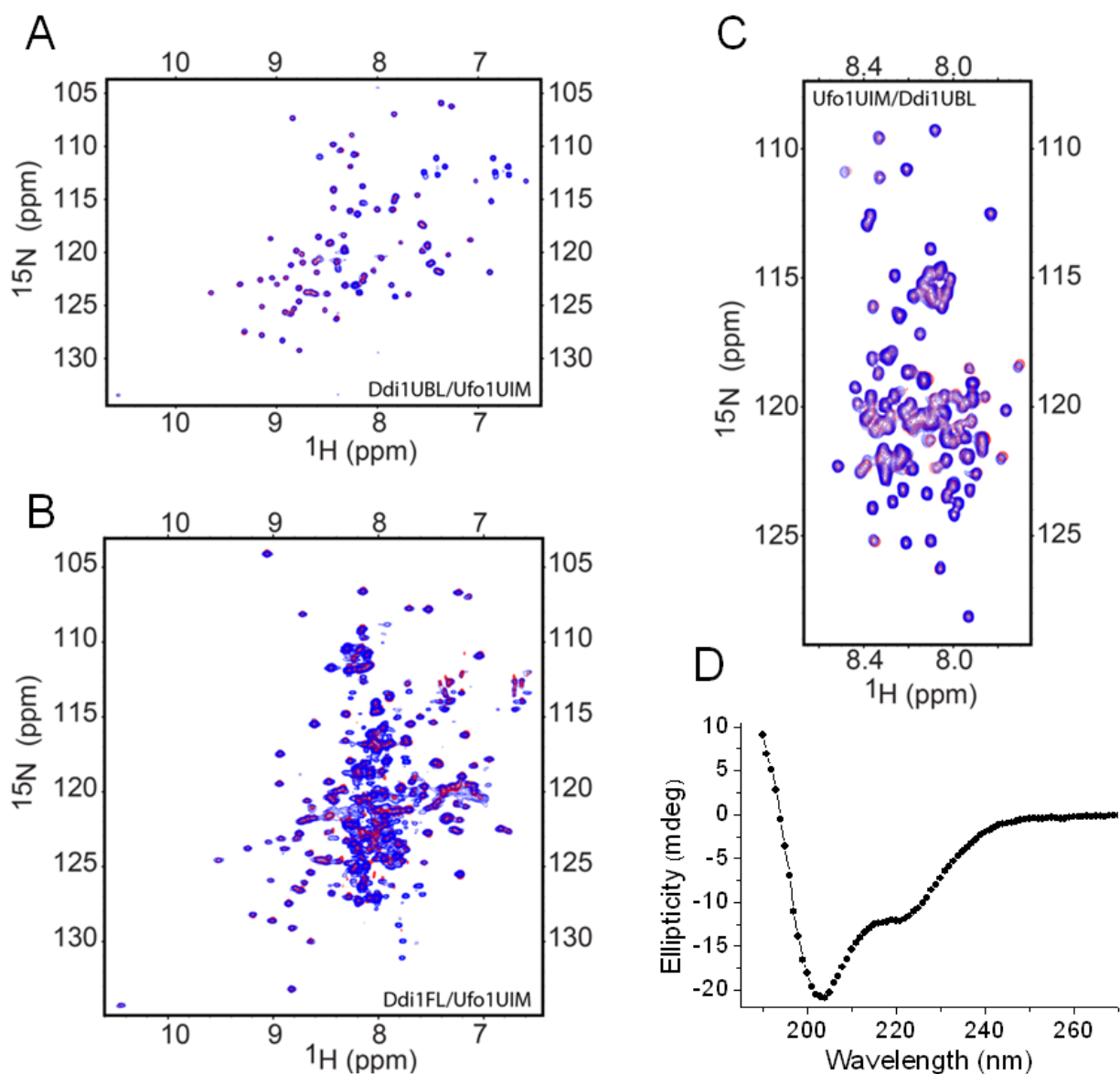
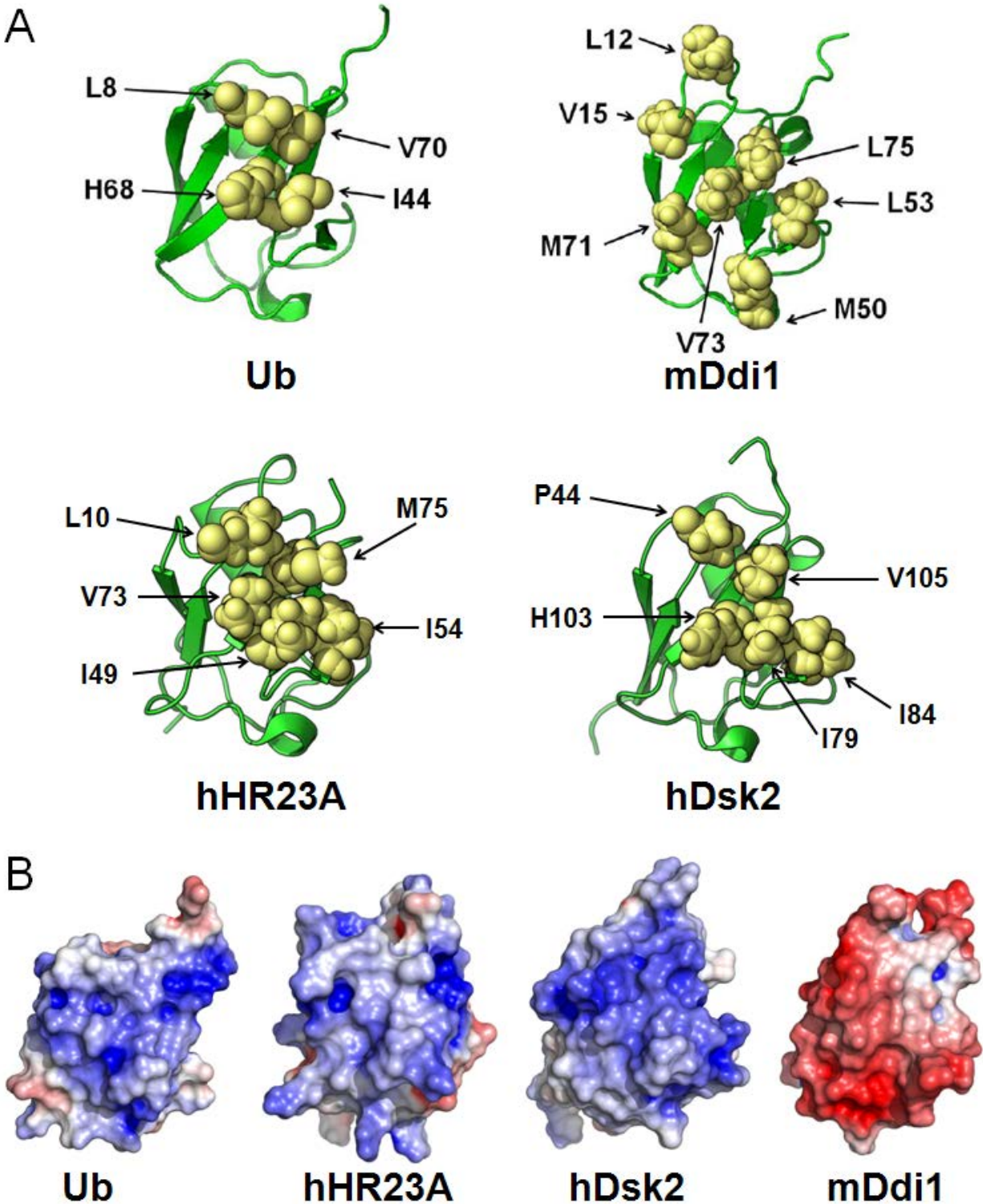


Figure S8, related to Figure 8. NMR analysis of the interaction between Ufo1UIMs and Ddi1 (FL or UBL). (A) Overlay of the  $^1\text{H}$ - $^{15}\text{N}$  SOFAST-HMQC spectra of  $^{15}\text{N}$ -labeled Ddi1UBL alone (red) and upon saturation (blue) with Ufo1UIM at 10-fold molar excess. (B) Overlay of the  $^1\text{H}$ - $^{15}\text{N}$  TROSY spectra of  $^{15}\text{N}$ -labeled FL Ddi1 alone (red) and saturated (blue) with Ufo1UIM, also at 10-fold molar excess. (C) Overlay of the  $^1\text{H}$ - $^{15}\text{N}$  SOFAST-HMQC spectra of  $^{15}\text{N}$ -labeled Ufo1UIM alone (red) and when saturated (blue) with Ddi1UBL at 10-fold molar excess. (D) Circular dichroism (CD) spectrum of Ufo1UIMs in 20 mM sodium phosphate buffer, pH 6.8, at 18°C, suggests the presence of  $\alpha$ -helical and some random-coil elements, in agreement with the prediction that Ufo1 contains UIM helices connected through unstructured linkers.



*Figure S9 related to Discussion.* Comparison of the structure and electrostatic potential of Ub and the UBL domains from mammalian proteasomal shuttle proteins Ddi1, Rad23, and Dsk2. (A) Solvent-exposed hydrophobic residues on the  $\beta$ -sheet side of the surface of Ub (PDB ID 1UBQ) and the UBL domains from mammalian proteins: a mouse protein homologous to Ddi1

(mDdi1; PDB 1V5O), human homologue of Rad23A (hHR23A; PDB ID 1P98), and human homologue of Dsk2 (aka ubiquilin-1 or hPLIC-1; PDB ID 2KLC). Structures of the backbone of these proteins are shown as green ribbons. Hydrophobic side chains are shown as yellow spheres and indicated with arrows. Note that 1V5O is the only structure of a UBL domain from a Ddi1 family protein currently available in the Protein Data Bank.

(B) Surface electrostatic potential of Ub (PDB ID 1D3Z) and the UBL domains from mammalian proteins: a mouse protein homologous to Ddi1 (mDdi1, PDB 1V5O), human homologue of Rad23A (hHR23A; PDB ID 1P98), and human homologue of Dsk2 (aka ubiquilin-1 or hPLIC-1; PDB ID 2KLC). Positive values of the potential are shown in blue while the negative values are red; the range is  $\pm 4$  kT/e for Ub and hHR23A,  $\pm 6$  kT/e for hDsk2 and mDdi1. All molecules are oriented similarly and such that the  $\beta$ -sheet surface faces the reader. The electrostatic potential map was generated as described in Figure S3B.

## Supplemental Tables

**Table S1, related to Figures 4 and 7. Active and passive residues in Ub and its binding partners used as input for computing the structures of Ub:Ddi1UBL and Ub:Ddi1UBA complexes using biomolecular docking program HADDOCK(de Vries et al., 2007; de Vries et al., 2010; Dominguez et al., 2003).**

| <b>Ub:Ddi1UBL Complex</b> |                  |   |
|---------------------------|------------------|---|
| <b>Ubiquitin</b>          | Active Residues  | 6,8,9,12,46,47,49,68,71,72,73                           |
|                           | Passive Residues | 2,10,14,39,44,48,51,52,64,74,75,76                      |
| <b>Ddi1UBL</b>            | Active Residues  | 4,8,11,12,15,17,48,49,50,53,66,67,68                    |
|                           | Passive Residues | 1,2,6,9,10,13,16,21,44,46,51,54,55,56,58,64,70,72,74,75 |
| <b>Ub:Ddi1UBA Complex</b> |                  |   |
| <b>Ubiquitin</b>          | Active Residues  | 6,8,10,42,44,47,48,49,68,70,71,73                       |
|                           | Passive Residues | 9,11,46,51,74   |
| <b>Ddi1UBA</b>            | Active Residues  | 400,401,402,420,423,424,427,428                         |
|                           | Passive Residues | 397, 404, 405, 406, 416, 421, 429                       |

Identification of active and passive residues was done based on the information from the NMR titration data (CSPs) combined with NACCESS (Hubbard and Thornton, 1993) analysis that allows quantification of the solvent accessibility of individual amino acids.

**Table S2, related to Figure 7. Unambiguous intermolecular distance constrains used as input for HADDOCK computation of the Ub:Ddi1UBL complex.**

| <b>PRE-based Distance Constraints for Ub:Ddi1UBL Complex</b> |                  |                |             |                |                |                |                      |
|--|------------------|----------------|-------------|----------------|----------------|----------------|----------------------|
| <b>Constraint ID #</b>                                       | <b>Protein</b>   | <b>Residue</b> | <b>Atom</b> | <b>Protein</b> | <b>Residue</b> | <b>Atom</b>    | <b>Distance, (Å)</b> |
| 1  | <b>Ubiquitin</b> | CYM            | OAH         | <b>Ddi1UBL</b> | 2              | H <sub>N</sub> | 15.84                |
| 2  |                  | CYM            | OAH         |                | 3              | H <sub>N</sub> | 16.07                |
| 3  |                  | CYM            | OAH         |                | 4              | H <sub>N</sub> | 15.39                |
| 4  |                  | CYM            | OAH         |                | 17             | H <sub>N</sub> | 17.75                |
| 5  |                  | CYM            | OAH         |                | 48             | H <sub>N</sub> | 14.51                |
| 6  |                  | CYM            | OAH         |                | 49             | H <sub>N</sub> | 15.02                |
| 7  |                  | CYM            | OAH         |                | 50             | H <sub>N</sub> | 16.71                |
| 8  |                  | CYM            | OAH         |                | 64             | H <sub>N</sub> | 15.97                |
| 9  |                  | CYM            | OAH         |                | 65             | H <sub>N</sub> | 12.84                |
| 10   |                  | CYM            | OAH         |                | 66             | H <sub>N</sub> | 11.14                |
| 11   |                  | CYM            | OAH         |                | 67             | H <sub>N</sub> | 9.95                 |
| 12   |                  | CYM            | OAH         |                | 68             | H <sub>N</sub> | 9.12                 |
| 13   |                  | CYM            | OAH         |                | 69             | H <sub>N</sub> | 11.3                 |
| 14   |                  | CYM            | OAH         |                | 70             | H <sub>N</sub> | 14.2                 |

These distance constraints were derived from paramagnetic relaxation enhancement (PRE) effects measured in Ddi1UBL as a result of paramagnetic spin-label (MTSL) attachment to cysteine at position 12 in Ub (Ub<sup>T12C,D77</sup>). The MTSL attached to C12 is denoted here as CYM residue.

## Supplemental Experimental Procedures

### Protein constructs and purification procedures

The Ddi1UBL construct used in these studies contains residues 2-80 of yeast Ddi1 (Uniprot P40087) flanked by a 12 amino-acid N-terminal His-tag (MRGSHHHHHHGS) and 3 amino-acid C-terminal extension (KLN). As both extensions are not part of Ddi1, the amino-acid numbering in the paper corresponds to the actual residue positions in Ddi1. Full-length Ddi1 (FL Ddi1), Dsk2UBL, Rad23UBL, and Ufo1UIMs (Uniprot Q04511, fragment containing residues 547-668 comprising three UIM motifs) constructs contained the same N-terminal His-tag for purification purposes. All UBL-containing constructs and FL Ddi1 were cloned in pQE30 vector (Qiagen) and expressed in M15 cells. Ufo1UIMs was cloned in pET28b (Novagen) and expressed in BL21(DE3)-Rosetta cells. All the above constructs were grown in LB media till  $A_{600}=0.6-0.8$  and induced with 1 mM IPTG for 6 h at 37°C or overnight at 20°C. Uniformly isotope-labeled ( $^{15}\text{N}$  or  $^{13}\text{C}/^{15}\text{N}$ ) proteins were grown in M9 minimal medium containing  $^{15}\text{NH}_4\text{Cl}$  or  $^{15}\text{NH}_4\text{Cl}$  and  $^{13}\text{C}_6\text{-D-glucose}$  and induced overnight at 20°C. Proteins were purified using 5 mL HiTrap Chelating HP Column followed by size exclusion separation on a Superdex 75 120 mL column. Expression and purification of human WT Ub and its variants, Ub<sup>T12C,D77</sup>, Ub<sup>K63C</sup>, Ub<sup>G75C</sup>, was performed as described elsewhere (Zhang et al., 2008).

The Ddi1UBA domain, containing amino acids 389 to 428 of yeast Ddi1 plus four extra residues, GSA at the N-terminus and S at the C-terminus, was cloned in pGEX4T2 vector and expressed in BL21(DE3)PlysS cells (Invitrogen). The unlabeled and  $^{15}\text{N}$  isotope labeled Ddi1UBA domain proteins were expressed using auto-inducing medium at 37°C (Studier, 2005). Purification of Ddi1UBA consists of several steps. After cell lysis, GST-tagged Ddi1UBA was separated using a 5 mL FF-GSTrap column. GST-tagged Ddi1UBA was then eluted out and dialyzed in PBS to remove glutathione. The GST tag was cleaved by incubation with thrombin overnight at 4°C. Ddi1UBA was purified using a 5 mL GSTrap column coupled with a 1 mL benzamidine column to remove both GST tags and thrombin. A Superdex 75 120 mL column was used at the end to remove residual GST tags.

### Sequence Analysis

All sequences used for analyses of Ddi1 gene structure can be found in the Uniprot Database under following ID numbers: Q8WTU0, Q95JI3, Q9DAF3, A0JPP7, F1MG01, A8B333, B9SX98, B9QR20, Q4UDI9, Q10256, Q5AY89, G3JEF4, Q2H085, Q54JB0. Sequence comparison was performed using ClustalW/ClustalOmega software available at EMBL-EBI webpage along with domain prediction software CDD and SMART (Goujon et al., 2010; Larkin et al., 2007; Letunic et al., 2012; Marchler-Bauer et al., 2013; Schultz et al., 1998; Sievers et al., 2011). Sequence alignment and quantification of sequence identity and similarity of Ddi1 UBA and UBL domains with human Ub (P0CG47), yeast Ub (P0CG63), Dsk2 (P48510), and Rad23 (P32628) was performed using EMBOSS software (Rice et al., 2000).

## **NMR experiments**

Final NMR samples were prepared in 20 mM sodium phosphate buffer, pH 6.8, 5% D<sub>2</sub>O, 0.02% NaN<sub>3</sub>, and, when indicated, 150 mM NaCl. In addition, FL Ddi1, Ddi1UBL, Rad23UBL samples and Cys mutants of Ub contained 3 mM TCEP. All NMR measurements were performed at 23°C on Avance III 600 MHz and 800 MHz Bruker Biospin spectrometers equipped with cryoprobes. The NMR data were processed using TopSpin 2.1 (Bruker Biospin) and analyzed using Sparky (Goddard and Kneller) or CARA (Keller, 2004; Keller, 2005) programs. <sup>1</sup>H-<sup>15</sup>N HSQC and TROSY spectra were acquired for verification of the full-length construct with individual domains. Triple-resonance NMR experiments: HNCO, HN(CA)CO, HN(CO)CA, HNCA, CBCA(CO)NH, HNCACB were used for <sup>13</sup>C', <sup>13</sup>C<sub>α</sub>, <sup>13</sup>C<sub>β</sub>, H<sub>N</sub>, and <sup>15</sup>N resonance assignment. CC(CO)NH, H(CCO)HN along with 2D and 3D TOCSY were used to obtain complete proton and carbon assignment. 2D and 3D NOESY spectra were collected and analyzed for Ddi1UBL and Ddi1UBA domains to obtain interproton NOE distance restraints. <sup>15</sup>N relaxation measurements (T<sub>1</sub>, hetNOE) were performed as described previously (Hall and Fushman, 2003). RDC measurements were performed in PEG/hexanol-based alignment medium (Ruckert and Otting, 2000) using IPAP-HSQC experiments (Ottiger et al., 1998) and analyzed using in-house program ALTENS (Varadan et al., 2002) to determine the alignment tensors.

## **NMR binding assays**

Binding assays were conducted by monitoring changes in the NMR signals of a <sup>15</sup>N-labeled protein upon titration of an unlabeled protein (ligand), as described (Varadan et al., 2005a). <sup>1</sup>H-<sup>15</sup>N SOFAST-HMQC spectra were collected and analyzed at each titration point, except for FL Ddi1 where <sup>1</sup>H-<sup>15</sup>N TROSY spectra were used. The starting protein concentration typically was around 250 μM or 600 μM (for some Ddi1UBA studies). The shifts in amide signals were quantified as chemical shift perturbations (CSP) using the following equation:  $\Delta\delta = [\Delta\delta_H^2 + (\Delta\delta_N/5)^2]^{0.5}$ , where  $\Delta\delta_H$  and  $\Delta\delta_N$  are chemical shift changes for <sup>1</sup>H and <sup>15</sup>N, respectively. The dissociation constants were obtained by fitting the titration data (CSPs versus concentrations of the binding partners) to various binding models using an in-house software KDFit as detailed elsewhere (Varadan et al., 2004). Best fit for Ub:DdiUBA and Ub:Ddi1UBL binding was obtained for a 1:1 stoichiometry model. In case of Ufo1UIMs binding to Ub, the best fit was obtained assuming that the three UIMs in Ufo1UIMs bind Ub independently and with similar affinities.

## **Ddi1UBL and Ddi1UBA domain structure calculations**

Structures of Ddi1 UBL and UBA domains were calculated using ARIA (Rieping et al., 2007) based on distance restraints from inter-proton NOEs, torsion angle constraints obtained from chemical shifts using TALOS+ (Cornilescu et al., 1999; Shen et al., 2009), hydrogen bonds (independently confirmed by H/D exchange experiments in case of Ddi1UBL), and NH-bond

orientation constrains derived from RDCs. RDCs were incorporated in the calculation only for the final structure refinement. Structures were validated by back-calculating RDC values from the derived structures using ALTENS (Varadan et al., 2002). The statistics are shown in Table 1 (main text).

### **Complex structure calculations**

Structures of Ub:Ddi1UBA and Ub:Ddi1UBL complexes were obtained using biomolecular docking program HADDOCK (de Vries et al., 2007; de Vries et al., 2010; Dominguez et al., 2003) and ambiguous interaction restraints generated from CSP-based mapping of the binding interfaces as well as unambiguous distance restraints obtained from site-directed spin labeling. The list of the active and passive residues used for each docking is in Table S1.

### **Site-directed spin labeling and paramagnetic relaxation enhancement (PRE) measurements**

Site-directed spin labeling was employed to generate unambiguous intermolecular distance constraints for determining the structure of Ub:Ddi1UBA and Ub:Ddi1UBL complexes or to independently verify the derived structures. The paramagnetic spin label, 1-oxyl-2,2,5,5-tetramethyl-3-pyrroline-3-methyl methanesulfonate (MTSL), was attached to a Cys at position 12, 63, or 75 in Ub, introduced via site-directed mutagenesis, as described (Varadan et al., 2005a; Varadan et al., 2004). The paramagnetic relaxation enhancement (PRE) effects in  $^{15}\text{N}$ -labeled Ddi1UBA or Ddi1UBL caused by MTSL attached to unlabeled Ub were quantified as the ratio of the signal intensities in the  $^1\text{H}$ - $^{15}\text{N}$  HSQC spectra of Ddi1UBA or Ddi1UBL recorded with MTSL in the oxidized and reduced states, as described (Varadan et al., 2005a; Zhang et al., 2008). All PRE measurements for  $^{15}\text{N}$ -labeled Ddi1UBL were performed in the presence of an equimolar amount of Ub $^{\text{T}12\text{C}}$ -MTSL, Ub $^{\text{K}63\text{C}}$ -MTSL, or Ub $^{\text{G}75\text{C}}$ -MTSL. PRE data analysis, including reconstruction of the MTSL position on Ub and distance determination was performed using program SLFIT (Ryabov and Fushman, 2006). The distance information obtained from PRE measurements with Ub $^{\text{T}12\text{C}}$ -MTSL was used to generate distance constraints for Ddi1UBL-Ub docking, summarized in Table S2. The PREs measured with Ub $^{\text{G}75\text{C}}$ -MTSL and Ub $^{\text{K}63\text{C}}$ -MTSL were not included in the structure calculation and instead used as positive and negative controls, respectively, to validate the computed structure. The PRE measurements for  $^{15}\text{N}$ -labeled Ddi1UBA were performed in the presence of approximately equimolar amount of Ub $^{\text{T}12\text{C}}$ -MTSL or in a 3-fold molar excess of Ub $^{\text{G}75\text{C}}$ -MTSL. These PREs were used to determine the relative orientation of Ddi1UBA and Ub, as discussed elsewhere (Zhang et al., 2008). The position of the MTSL's unpaired electron reconstructed from the PREs measured in Ddi1UBA was used to generate loose intermolecular distance restraints between a selected residue in Ddi1UBA and the  $\text{C}_\alpha$  of the respective cysteine in Ub, for HADDOCK calculation.

## Circular dichroism measurements

The CD spectra were measured on Jasco J-810 spectropolarimeter in continuous mode with 100 nm/min scanning speed, 4 sec response, 2 nm bandwidth, and 10 mm path length. Ufo1UIMs construct was at 4.5  $\mu\text{M}$  concentration in 20mM sodium phosphate buffer at pH 6.8. Ellipticity was monitored in the range of 190-340 nm at 18°C.

## Small-angle neutron scattering (SANS) measurements

SANS measurements were performed at the NIST Center for Neutron Research (NCNR). An equimolar mixture of Ddi1UBL and Ub (total concentration 5.11 mg/mL) in a D<sub>2</sub>O buffer (pD 6.8) containing 20 mM sodium phosphate and 3 mM TCEP was loaded into demountable 2 mm path length quartz cuvette and measured at 23°C. SANS was also measured separately for samples of isolated Ddi1UBL (4.69 mg/mL) and Ub (4.5 mg/mL). The neutron wavelength,  $\lambda$ , was 6 Å, with a wavelength spread,  $\Delta\lambda/\lambda$ , of 0.15. Scattered neutrons were detected with a 64 cm x 64 cm two-dimensional position-sensitive detector with 128 x 128 pixels at a resolution of 0.5 cm/pixel. The data were reduced and analyzed as described (Castaneda et al., 2013) to produce scattered intensity,  $I(q)$ , versus  $q$ , where  $q = 4\pi \sin(\theta)/\lambda$  and  $2\theta$  is the scattering angle.

## Comparison of NMR-derived structures with SANS data

In order to account for the flexible N- and C-termini of the Ddi1UBL construct used in these studies but not present in the NMR-derived structures, the corresponding MRGSHHHHHHGS and KLN residues were built at the N- and C-termini, respectively, of the UBL structure by using the Modeller software (Eswar et al., 2006; Marti-Renom et al., 2000). To account for the possible conformational space sampled by the UBL's tails, 1609 conformations of Ddi1UBL and 500 conformations of the Ub:Ddi1UBL complex were generated using the Monte Carlo module of the SASSIE software (Curtis et al., 2012), starting from the averaged docked structure. For each generated conformer, only 12 residues of the N-terminus and 8 residues of the C-terminus of this extended Ddi1UBL construct were allowed to explore the conformational space. For each generated structure of the complex, the corresponding  $I(q)$  was computed from the atom coordinates using the Xtal2sas module of SASSIE, and assuming 100% deuterated solvent and protonated protein with no hydration layer. The calculated scattering intensities for each conformer (1609 for Ddi1UBL or 500 for Ub:Ddi1UBL) were averaged, and the resulting  $I(q)$  was compared with the experimental data (see Figure S7F,G) as described below.

In the case of free Ddi1UBL, the scaling factor,  $w$ , between the calculated,  $I(q)^{calc}$ , and experimental,  $I(q)$ , intensities was obtained by least-squares minimization of the difference between  $I(q)$  and  $w I(q)^{calc}$ . The agreement between the experiment and calculation is shown in Figure S7F.

To account for the contributions to neutron scattering from the unbound Ddi1UBL and Ub which are present in the Ddi1UBL+Ub sample during SANS measurements, we implemented the following procedure. The scattering intensity of the Ddi1UBL+Ub sample was considered as the sum of the scattering by the Ddi1UBL/Ub complex and the scattering by the unbound Ddi1UBL and Ub, which we represent using the following equation:

$$I(q)^{total} = w_C I(q)^{calc,complex} + w_{UBL} I(q)^{expt,UBL} + w_{Ub} I(q)^{expt,Ub}. \quad (S1)$$

Here  $I(q)^{calc,complex}$  is the scattering intensity for Ddi1UBL:Ub complex (calculated directly from the structure of the complex as detailed in the previous paragraph),  $I(q)^{expt,UBL}$  and  $I(q)^{expt,Ub}$  are the experimental scattering intensities for Ddi1UBL and Ub, respectively, measured separately for the isolated proteins,  $w_{Ub}$  is the scaling coefficient equal to the ratio of molar concentrations of unbound Ub in the Ddi1UBL+Ub sample and in the isolated-Ub sample,  $w_{UBL}$  represents the same for Ddi1UBL, and  $w_C$  is the scaling factor that relates the predicted and experimental values for Ddi1UBL:Ub complex. Note that the molar concentrations of the unbound Ub and Ddi1UBL in the Ddi1UBL+Ub sample were assumed to be equal, to reflect the equimolar amounts of each protein present in the sample, and the 1:1 stoichiometry of the complex. Therefore,  $w_{UBL} = \kappa w_{Ub}$ , where  $\kappa$  is a fixed coefficient that merely reflects the difference in the molar concentrations of the isolated Ub and UBL in the corresponding samples/measurements. Because of the arbitrary scale of the predicted  $I(q)$  values,  $I(q)^{calc,complex}$  was scaled prior to the analysis, to make its lowest- $q$  value match that of the experimental  $I(q)$ . We verified by using different initial scalings for  $I(q)^{calc,complex}$  that they had no effect on the resulting agreement between the experimental  $I(q)$  and fitted values of  $I(q)^{total}$  or the value of  $w_{Ub}$  (in “calculation 2”, see below).

The following two approaches were used for the analyses.

Calculation 1. The coefficients  $w_{Ub}$  and  $w_{UBL}$  ( $= \kappa w_{Ub}$ ) were calculated as the ratio of molar concentrations of unbound Ub (or UBL) in the Ddi1UBL+Ub sample and in the isolated-Ub (or isolated-UBL) sample. The concentration of the unbound species in the Ddi1UBL+Ub sample was determined based on the total concentrations of Ub and UBL in the Ddi1UBL+Ub sample and the NMR-derived  $K_d$  value (45  $\mu\text{M}$ ) using the following equation (for 1:1 binding) (Varadan et al., 2004):

$$[Ub] = \frac{-([UBL_t] - [Ub_t] + K_d) + \sqrt{([UBL_t] + [Ub_t] + K_d)^2 + 4[Ub_t]K_d}}{2}, \quad (S2)$$

where  $[Ub]$  is the molar concentration of unbound Ub, and  $[Ub_t]$  and  $[UBL_t]$  are the total molar concentrations of the corresponding proteins.

With  $w_{Ub}$  and  $w_{UBL}$  fixed,  $w_C$  is the only adjustable parameter in Eq (S1); its value was obtained by a least-squares minimization of the difference between  $I(q)$  and  $I(q)^{total}$ . In our case  $[Ub] = 89 \mu\text{M}$ ,  $\kappa = 1.2$ ,  $w_{Ub} = 0.169$ , and  $w_{UBA} = 0.203$ . The fitting gave  $w_C = 0.761 \pm 0.003$  and  $\chi^2 = 79.1$ .

Note that  $\chi^2 = \sum_i \left[ \frac{I(q_i) - I(q_i)^{total}}{\sigma(q_i)} \right]^2$ , where  $\sigma(q)$  is the experimental error in  $I(q)$ .

**Calculation 2.** In order to find out if the agreement between  $I(q)$  and  $I(q)^{total}$  can be improved further by varying  $w_{Ub}$ , we treated the coefficient  $w_{Ub}$  as a fitting parameter together with  $w_C$  (recall that  $w_{UBL} = \kappa w_{Ub}$  where  $\kappa$  is fixed). The analysis gave  $w_{Ub} = 0.127 \pm 0.007$ ,  $w_C = 0.832 \pm 0.012$ , and  $\chi^2 = 41.8$ , indicating an improvement in the agreement.

The agreement between the experimental  $I(q)$  and  $I(q)^{total}$  for both calculations is shown in Figure S7G.

The resulting value of  $w_{Ub}$  from Calculation 2 corresponds to molar concentration of  $67 \pm 4 \mu\text{M}$  for the unbound Ub and UBL, and the dissociation constant of  $\sim 23 \pm 3 \mu\text{M}$ . While clearly a rough estimate, these values of [Ub] and  $K_d$  are comparable to the corresponding values calculated from the NMR-derived parameters (see Calculation 1).

### **Pull-down assays**

60  $\mu\text{g}$  of purified recombinant RGS-His<sub>6</sub>-Ddi1UBL or His<sub>6</sub>-Ub were incubated with activated CH-sepharose beads overnight at 4°C. The beads were washed with PBS buffer, the remaining active groups were blocked with primary amines-containing buffer (100 mM Tris pH 8.0 or 1M Ethanolamine pH 8.0). After that they were vigorously washed with buffers of alternating pH (0.1 M Acetic acid, 0.5 M NaCl and 0.1 M Tris-HCl buffer pH 8.0, 0.5 M NaCl) and were re-equilibrated with Binding Buffer (50 mM phosphate buffer, pH 7.4, 150 mM NaCl, 1% Triton X-100, 0.2 mg/ml BSA, 5 mM EDTA). 50  $\mu\text{g}$  of RGS-His<sub>6</sub>-Ddi1UBL were incubated for 2 hours at 4°C with Ddi1UBL-beads, Ub-beads, or empty beads (all treated same). Unbound proteins were washed out with TBS buffer (50 mM Tris-HCl pH 8.0, 150 mM NaCl). Elution was performed by beads boiling with 2X Laemmli protein sample buffer. Eluted proteins were separated on 16% Tris-Tricine PAGE and immunoblotted with anti-RGS antibody (Qiagen). Pull-out of polyUb conjugates on Ddi1UBL or Ub column was performed in a similar manner with the exception that 0.7 mg of purified RGS-His<sub>6</sub>-Ddi1UBL or His<sub>6</sub>-Ub were used to attach to CH-sepharose beads. *DDI1* yeast cells were grown in YPD media to  $\text{OD}_{A600} \sim 2.7$  and harvested. Obtained pellet was re-suspended in Binding Buffer supplemented with 5 mM ATP, PI cocktail, and 50  $\mu\text{M}$  MG132. The cells were broken by vortexing 10 min at 4°C with glass beads and the lysate was clarified by centrifugation. 12.9 mg of total protein extract were incubated for 2 hours at 4°C with Ddi1UBL-beads, Ub-beads, or empty beads. Unbound proteins were removed by vigorous wash with TBS buffer. Elution was performed by incubation with 8M urea containing buffer for 10 min at 45°C. Eluted proteins were TCA precipitated, then resuspended in 2X Laemmli protein sample buffer, resolved on 16% Tris-Tricine PAGE, and immunoblotted with anti-Ub antibody (Dako).

## Supplemental References

Castaneda, C.A., Kashyap, T.R., Nakasone, M.A., Krueger, S., and Fushman, D. (2013). Unique structural, dynamical, and functional properties of K11-linked polyubiquitin chains. *Structure* *21*, 1168-1181.

Clore, G., and Garrett, D. (1999). R-factor, free R, and complete cross-validation for dipolar coupling refinement of NMR structures. *J Am Chem Soc* *121*, 9008-9012.

Cornilescu, G., Delaglio, F., and Bax, A. (1999). Protein backbone angle restraints from searching a database for chemical shift and sequence homology. *J Biomol NMR* *13*, 289-302.

Curtis, J.E., Raghunandan, S., Nanda, H., and Krueger, S. (2012). SASSIE: A program to study intrinsically disordered biological molecules and macromolecular ensembles using experimental scattering restraints. *Comput Phys Commun* *183*, 382-389; software available at: [http://www.smallangles.net/sassie/SASSIE/SASSIE\\_HOME.html](http://www.smallangles.net/sassie/SASSIE/SASSIE_HOME.html).

de Vries, S.J., van Dijk, A.D., Krzeminski, M., van Dijk, M., Thureau, A., Hsu, V., Wassenaar, T., and Bonvin, A.M. (2007). HADDOCK versus HADDOCK: new features and performance of HADDOCK2.0 on the CAPRI targets. *Proteins* *69*, 726-733.

de Vries, S.J., van Dijk, M., and Bonvin, A.M. (2010). The HADDOCK web server for data-driven biomolecular docking. *Nat Protoc* *5*, 883-897.

Dolinsky, T.J., Nielsen, J.E., McCammon, J.A., and Baker, N.A. (2004). PDB2PQR: an automated pipeline for the setup of Poisson-Boltzmann electrostatics calculations. *Nucleic Acids Res* *32*, W665-667.

Dominguez, C., Boelens, R., and Bonvin, A.M. (2003). HADDOCK: a protein-protein docking approach based on biochemical or biophysical information. *J Am Chem Soc* *125*, 1731-1737.

Eswar, N., Webb, B., Marti-Renom, M.A., Madhusudhan, M.S., Eramian, D., Shen, M.Y., Pieper, U., and Sali, A. (2006). Comparative protein structure modeling using Modeller. *Curr Protoc Bioinformatics Chapter 5*, Unit 5 6.

Goddard, T.D., and Kneller, D.G. SPARKY 3, University of California, San Francisco.

Goujon, M., McWilliam, H., Li, W., Valentin, F., Squizzato, S., Paern, J., and Lopez, R. (2010). A new bioinformatics analysis tools framework at EMBL-EBI. *Nucleic Acids Res* *38*, W695-699.

Hall, J.B., and Fushman, D. (2003). Characterization of the overall and local dynamics of a protein with intermediate rotational anisotropy: Differentiating between conformational exchange and anisotropic diffusion in the B3 domain of protein G. *J Biomol NMR* *27*, 261-275.

Hubbard, S., and Thornton, J. (1993). 'NACCESS', computer program, Department of Biochemistry and Molecular Biology, University College London.

Keller, R. (2004). *The Computer Aided Resonances Assignment Tutorial*, First edn (CANTINA Verlag).

Keller, R. (2005). *Optimizing the process of nuclear magnetic resonance spectrum analysis and computer aided resonance assignment* (Thèse de doctorat, ETH Zurich Thesis No. 15947, Switzerland).

Larkin, M.A., Blackshields, G., Brown, N.P., Chenna, R., McGettigan, P.A., McWilliam, H., Valentin, F., Wallace, I.M., Wilm, A., Lopez, R., *et al.* (2007). Clustal W and Clustal X version 2.0. *Bioinformatics* 23, 2947-2948.

Letunic, I., Doerks, T., and Bork, P. (2012). SMART 7: recent updates to the protein domain annotation resource. *Nucleic Acids Res* 40, D302-305.

Marchler-Bauer, A., Zheng, C., Chitsaz, F., Derbyshire, M.K., Geer, L.Y., Geer, R.C., Gonzales, N.R., Gwadz, M., Hurwitz, D.I., Lanczycki, C.J., *et al.* (2013). CDD: conserved domains and protein three-dimensional structure. *Nucleic Acids Res* 41, D348-352.

Marti-Renom, M.A., Stuart, A.C., Fiser, A., Sanchez, R., Melo, F., and Sali, A. (2000). Comparative protein structure modeling of genes and genomes. *Annu Rev Biophys Biomol Struct* 29, 291-325.

Ottiger, M., Delaglio, F., and Bax, A. (1998). Measurement of J and dipolar couplings from simplified two-dimensional NMR spectra. *J Magn Reson* 131, 373-378.

Pymol. The Pymol Molecular Graphics System, Version 1.2r1 (Schrödinger, LLC.).

Rice, P., Longden, I., and Bleasby, A. (2000). EMBOSS: the European Molecular Biology Open Software Suite. *Trends Genet* 16, 276-277.

Rieping, W., Habeck, M., Bardiaux, B., Bernard, A., Malliavin, T.E., and Nilges, M. (2007). ARIA2: automated NOE assignment and data integration in NMR structure calculation. *Bioinformatics* 23, 381-382.

Ruckert, M., and Otting, G. (2000). Alignment of biological macromolecules in novel nonionic liquid crystalline media for NMR experiments. *J Amer Chem Soc* 122, 7793-7797.

Ryabov, Y., and Fushman, D. (2006). Interdomain mobility in di-ubiquitin revealed by NMR. *Proteins* 63, 787-796.

Schultz, J., Milpetz, F., Bork, P., and Ponting, C.P. (1998). SMART, a simple modular architecture research tool: identification of signaling domains. *Proc Natl Acad Sci U S A* 95, 5857-5864.

Shen, Y., Delaglio, F., Cornilescu, G., and Bax, A. (2009). TALOS+: a hybrid method for predicting protein backbone torsion angles from NMR chemical shifts. *J Biomol NMR* 44, 213-223.

Sievers, F., Wilm, A., Dineen, D., Gibson, T.J., Karplus, K., Li, W., Lopez, R., McWilliam, H., Remmert, M., Söding, J., *et al.* (2011). Fast, scalable generation of high-quality protein multiple sequence alignments using Clustal Omega. *Mol Syst Biol* 7, 539.

Studier, F.W. (2005). Protein production by auto-induction in high density shaking cultures. *Protein Expr Purif* 41, 207-234.

Varadan, R., Assfalg, M., and Fushman, D. (2005a). Using NMR spectroscopy to monitor ubiquitin chain conformation and interactions with ubiquitin-binding domains. In *Ubiquitin and Protein Degradation, Methods in Enzymology*, Vol 399 part B, R.J.Deshaies, ed., pp. 177-192.

Varadan, R., Assfalg, M., Haririnia, A., Raasi, S., Pickart, C., and Fushman, D. (2004). Solution conformation of Lys63-linked di-ubiquitin chain provides clues to functional diversity of polyubiquitin signaling. *J Biol Chem* 279, 7055-7063.

Varadan, R., Assfalg, M., Raasi, S., Pickart, C., and Fushman, D. (2005b). Structural determinants for selective recognition of a Lys48-linked polyubiquitin chain by a UBA domain. *Mol Cell* 18, 687-698.

Varadan, R., Walker, O., Pickart, C., and Fushman, D. (2002). Structural properties of polyubiquitin chains in solution. *J Mol Biol* 324, 637-647.

Zhang, D., Raasi, S., and Fushman, D. (2008). Affinity makes the difference: nonselective interaction of the UBA domain of Ubiquitin-1 with monomeric ubiquitin and polyubiquitin chains. *J Mol Biol* 377, 162-180.